JCTC Journal of Chemical Theory and Computation

Article

pubs.acs.org/JCTC

Role of Solvent on Charge Transfer in 7-Aminocoumarin Dyes: New Hints from TD-CAM-B3LYP and State Specific PCM Calculations

Alfonso Pedone*

†Department of Chemical and Geological Sciences, University of Modena and Reggio Emilia, via G. Campi 183, I-41125, Modena, Italy

ABSTRACT: Time-dependent B3LYP and CAM-B3LYP calculations have been used to investigate the absorption and emission energies as well as to shed light on the formation of the twisted intramolecular charge transfer state (TICT) in Coumarin-152 (C152) embedded in cyclohexane, acetonitrile, and water solvents. The bulk solvent effects have been included by using the linear-response (LR) and State-Specific (SS) models in the framework of the so-called polarizable continuum method (PCM). The results demonstrate that the choice of the exchange-correlation functional and of the PCM model is critical to reproduce the experimental data in the most accurate way. In particular, it has been observed that both the solvatochromic and Stokes' shifts are well reproduce by CAM-B3LYP/SSPCM calculations performed on the S_0 and S_1 geometries of C152 optimized at the B3LYP/LRPCM level of theory, whereas not accurate Stokes' shifts are computed with CAM-B3LYP/SSPCM calculations carried out on the CAM-B3LYP/LRPCM optimized structures. This is attributed to the incorrect (underestimated) solvation energy provided by LRPCM, which could lead to misleading results especially for charge-transfer excited state structures in polar solvents. Instead, B3LYP/LRPCM excited state optimizations seem to provide a reasonable geometry for a simple '*error cancellation*' effect due to the balance among the B3LYP overstabilization of charge transfer states and the LRPCM underestimation of the solute−solvent binding energy when the former is in a polar solvent. Finally, CAM-B3LYP/SSPCM calculations, in very good agreement with experimental evidence, show that the formation of an accessible TICT state is possible for C152 and that the crossing between S_0 and S_1 states at a dihedral angle of around 70° occurs only in polar solvents.

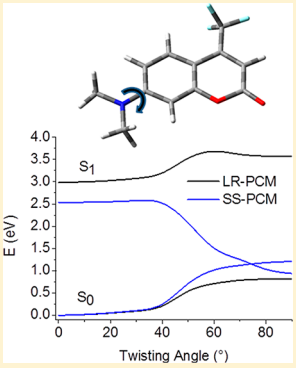

INTRODUCTION

Coumarin dyes having different amino groups at 7-position (commonly known as 7-aminocoumarins) are widely used as laser dyes in the blue-green region[1,2] and studied for their applicability as organic semiconductor materials, optical memory materials and optical sensors when conjugated to polymeric thin films[3] or encapsulated in silica matrix.[4]

These molecules show a substantial difference between the ground and excited state dipole moments, strongly polarity dependent Stokes shifts, and very high fluorescent quantum yields.[5,6] All these properties have made coumarin dyes useful fluorescent probes for the investigation of several chemical and photochemical processes occurring in different homogeneous (solvents and mixture of solvents) or heterogeneous environments (micelles, polymer, and inorganic solids).[7]

As a consequence of the wide range of applicability of coumarin dyes, their photophysical properties have been subjected to extensive investigations for quite a long time.[8,9] However, in spite of the relevant number of literature reports, many of the photophysical properties of these molecules are still unclear and thus debated.[5,6,10,11]

Several investigations have shown that coumarin dyes having simple 7-NH_2 substituent have unusually lower fluorescent quantum yields (Φ_F) and fluorescence lifetimes (τ_F) in nonpolar solvent in comparison with those observed in other solvents of moderate to high polarities.[6,12]

The unusual fluorescent quenching in nonpolar solvent was claimed to be due to the existence of a pyramidal structure of the $-NH_2$ moiety in nonpolar solvents compared to the planar structure, able to give intramolecular charge transfer (ICT), which is hypothesized to exist in polar solvents.

Instead, an opposite behavior has been observed for 7-aminocoumarin dyes in which the two hydrogen atoms are substituted by two alkyl groups.[5,10] In fact, high values of fluorescence quantum yields and lifetimes are observed in apolar solvents, whereas these values are drastically reduced and become strongly temperature dependent in polar solvents.

This behavior has been attributed to the formation of a nonemissive twisted intramolecular charge transfer (TICT) state in highly polar solvents that allows for a fast nonradiative de-excitation of the dye molecule to the ground state.[5,10]

Therefore, the understanding of the solvent and environment effects causing the presence/absence of the TICT state in 7-aminocoumarins is of primary importance to design new molecular systems with specific photophysical properties.

To this end, theoretical models able to provide insights into the properties of electronically excited states are becoming useful tools to complement the indirect information obtained through experimental measurements.

Received: May 27, 2013
Published: August 1, 2013

Time-Dependent Density Functional Theory (TDDFT)[13,14] is the most effective and thus widely used approach to investigate the excited state properties and optical spectra of medium- to large-size organic molecules in gas phase, solution, or even in more complex environments.[15−26]

For the specific case of coumarin derivatives, several TDDFT investigations have been carried out in the past with the aim of computing the vertical absorption and the fluorescence emission energies of the Intramolecular Charge Transfer (ICT) state of ($\pi\pi^*$) character,[21,27−31] the vibronic spectra[32] or the excited state hydrogen bonding dynamics of photo-excited coumarins in aqueous solvents.[33,34]

Most of these works showed that global hybrid functional such as B3LYP[35] and PBE0[36] provide the best results in term of vertical excitation energies.

However, to the best of our knowledge, none of the previously published papers was dedicated to the understanding of the de-excitation mechanism of 7-amino coumarin molecules in different solvents and especially to the important issue of how the solvent rules the relative stability among the ICT and the TICT states.

This is the aim of the present contribution in which TDDFT calculations coupled with the Polarizable Continuum Method (PCM)[37] have been employed to accounts for the effect of aprotic (cyclohexane (CHX) and acetonitrile (ACN)) and protic (water (WAT)) solvents on the formation of the TICT state in C152 whose chemical structure is shown in Scheme 1.

Scheme 1. Chemical Structure of Coumarin-152 (C152)

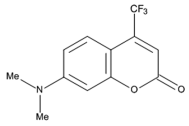

It is well-known that the reliability of the TDDFT results strongly depends on the choice of the exchange-correlation functional. For instance, previous studies have demonstrated that the accurate quantification of the relative stability of twisted and planar intramolecular charge transfer states is an impossible task for pure-GGA and hybrid functionals.[38−40] In fact, they suffer from overpolarization of charge transfer states for which a small spatial overlap between the occupied and virtual orbitals involved in the transition is present. To overcome this problem long-range separated hybrid functional such as the CAM-B3LYP must be used since it has been demonstrated to better describe charge transfer excited states than the global hybrid B3LYP functional.[40]

However, in the calculation of excited state properties of organic molecules in solution a further source of inaccuracy can derive from the choice of the PCM model used to include solvent effects, especially for charge transfer states in polar solvents. Two methods have been devised to account for solvent effects during TDDFT calculations: conventional linear response (LR) and state specific (SS) approaches.[41,42] These are intrinsically different since in SS approaches the solvent reaction field is computed (in a self-consistent way) by using the electron density of the state of interest, while in LR the absorption/emission energies are computed as poles of the frequency dependent response functions of the ground electronic state avoiding explicit calculation of the excited state wave function. The latter approach is more often used in standard TDDFT/PCM calculations because it is computationally cheaper, and since analytical gradients are available, it allows performing excited state geometry optimizations and vibrational frequencies calculations.[43] However, LRPCM provides a less rigorous treatment of dynamical solvent effects and a less balanced description of strong and weak electronic transitions, and it tends to under stabilize charge transfer states.[41,42,44]

On the contrary, SS calculations provide more reliable and accurate excited state energies of molecular systems in solution, but excited state analytical gradients are not yet available. This is certainly a big issue since, as recently shown by Improta[45] for DNA nucleobases, LRPCM geometry optimizations using the CAM-B3LYP functional can lead to erratic minima of the states with CT character since their energy is underestimated by LRPCM whereas global-hybrid functional could yield better CT geometries for a simple error cancellation.

THEORETICAL BACKGROUND: THE POLARIZABLE CONTINUUM MODEL

The polarizable continuum model (PCM)[37] describes the solvent as a homogeneous dielectric medium, which is polarized by the solute. The latter is placed within a cavity in the solvent that is built as the envelope of spheres centered on the solute atoms on which a classical electrostatic problem (the Poisson equation):

$$-\nabla\cdot[\varepsilon(r)\nabla V(r)] = 4\pi\rho_M(r) \tag{1}$$

is solved using a boundary element approach.[37]

In this equation, ε is the permittivity, ρ_M is the solute charge distribution, and V is an electrostatic potential given by the sum of solute potential plus the contribution given by the reaction of the solvent, that is, the polarization of the dielectric.

The reaction potential is described by an apparent charge distribution placed at the center of small tiles (surface tesserae) that subdivide the cavity surface and interact with the solute electrostatic potential providing the following solvent induced contribution to the free energy (G):

$$G = \frac{1}{2}\boldsymbol{V}^T\boldsymbol{q} \tag{2}$$

where $\boldsymbol{V}$ is a vector collecting the values of the electrostatic potential and $\boldsymbol{q}$ contains the apparent surface charges which depend on the solute's electrostatic potential through the general equation $\boldsymbol{q} = -\boldsymbol{D}\boldsymbol{V}$ where the square matrix $\boldsymbol{D}$ is related to the geometry of the cavity and the solvent dielectric constant.

When studying electronic processes such as the formation and/or relaxation of excited states in solution the delay response of the solvent (that is, the solvent dynamics) with respect to the ultrafast time scale of the excitation/de-excitation processes have to be taken in the proper account. The PCM approach involves the definition of two limit time regimes, the equilibrium (EQ) and the nonequilibrium (NEQ) one. In the former, all the electronic and the nuclear solvent degrees of freedom are in equilibrium with the electron density of the solute and the apparent surface charges are computed by employing the static dielectric constant. In the latter, only the solvent electronic polarization is in equilibrium with the excited-state electron density, and the apparent surface charges are split into two set of charges representing the fast (electronic) and slow (inertial) components whose values are

computed by using the optical and static dielectric constants, respectively.

In absorption processes, the solvent is in nonequilibrium with the new excited electron density and the vertical excitation energy is computed by the following relationship:

$$\Delta G_{abs} = G^{1}_{neq} - G^{0}_{eq} \tag{3}$$

where G^{1}_{neq} and G^{0}_{eq} are the nonequilibrium excited state and the equilibrium ground state free energies, respectively.

After the electronic transition, the molecule starts to relax toward the excited state potential energy minimum. At the same time, the solvent molecules start to reorient in order to reach the equilibrium with the excited state electron density. Since these two processes cannot be rigorously decoupled, especially when they exhibit similar time scales there is not a suitable single strategy to investigate all the possible emission processes.

However, in many cases, the equilibration of intramolecular degrees of freedom is faster than solvent equilibration, and it can be assumed that the emission occurs from the excited state minimum. This is especially true for coumarin molecules in polar solvent whose electronic transitions involve significant variations of the excited state electron density.

For molecules presenting ultrafast excited state decay, only the fast solvent degrees of freedom are in equilibrium with the excited state density and the ΔG_{emi} can be computed in the same way as ΔG_{abs} after having relaxed the excited state geometry at the nonequilibrium level.

Instead, for molecules with very long excited state lifetimes, as in the case of coumarin derivatives, it is possible to assume that all the solvent degrees of freedom are in equilibrium with the excited state density and the fluorescence can be computed by

$$\Delta G_{emi} = G^{1}_{eq} - G^{0}_{neq} \tag{4}$$

where G^{1}_{eq} and G^{0}_{neq} are the equilibrium excited state and the nonequilibrium ground state free energies, respectively.

In the State-Specific PCM implementation[41,42] the excited state equilibrium G^{1}_{eq} free energy in solution explicitly depends on the excited state:

$$G^{1}_{eq} = \frac{1}{2}\sum_{i} q^{(1)}_{i} V^{(1)}_{i,\rho} = \frac{1}{2}\sum_{i} q^{(1)}_{i,f} V^{(1)}_{i,\rho} + \frac{1}{2}\sum_{i} q^{(1)}_{i,s} V^{(1)}_{i,\rho} \tag{5}$$

whereas the nonequilibrium G^{1}_{neq} free energy explicitly depends also on the density of the ground state (0)

$$G^{1}_{neq} = \frac{1}{2}\sum_{i} q^{(1)}_{i,f} V^{(1)}_{i,\rho} + \left(\sum_{i} q^{(0)}_{i,s} V^{(1)}_{i,\rho} - \frac{1}{2}\sum_{i} q^{(0)}_{i,s} V^{(0)}_{i,\rho}\right) + \left(\frac{1}{2}\sum_{i} q^{(0)}_{i,s} V^{(1)}_{i,f} - \frac{1}{2}\sum_{i} q^{(0)}_{i,s} V^{(0)}_{i,f}\right) \tag{6}$$

Instead, the ground state nonequilibrium (G^{0}_{neq}) free energy in solution can be obtained by eq 6 but interchanging the labels (0) and (1).

In the above equations q_f/q_s and V_f/V_s are the polarization charges and the corresponding potentials related to the fast and slow solvent degree of freedom while $V^{(n)}_{i,\rho}$ is the potential generated by the density of the state n.

The calculations of the aforementioned quantities is performed by using a self-consistent iterative procedure as described by Improta and co-workers.[41,42]

As for the linear response formalism, the excitation energies are computed by solving the TDDFT equation in which the coupling matrix **K** is decomposed in two terms; one is related to the gas phase calculation and the other related to solvent. The PCM contribution to the TDDFT equations depends on an electrostatic potential ($\delta\varphi$) computed by using the electron density variation associated to the electronic transition in place of the specific electron density of the excited state:

$$\delta\varphi(s', \omega) = \int_{R^3} \frac{\delta\rho^{el}(r', \omega)}{|s' - r'|} dr' \tag{7}$$

and the PCM operator is defined as

$$v^{PCM}[\delta\rho^{el}](r) = \iint_{\Gamma} \delta\varphi(s', \omega) \frac{Q(\varepsilon; s', s)}{|s - r|} ds\, ds' \tag{8}$$

where the PCM response matrix Q depends on the dielectric constant at optical frequency in the nonequilibrium case and on the static dielectric constant in the equilibrium case. Finally, it is worth to remember that in LRPCM method the ground state is always fully equilibrated with the solvent degrees of freedom.

COMPUTATIONAL DETAILS

All QM calculations were performed at the DFT and/or TDDFT level of theory by using the Gaussian09 suite of programs.[46] The hybrid exchange−correlation functional B3LYP[35,47] and the long-range corrected CAM-B3LYP[48] functionals coupled to the polarized double-ζ N07D basis set have been employed.[49] The N07D basis set, which has been constructed by adding a reduced number of polarization and diffuse functions to the 6-31G set, leads to an accuracy at least comparable to the aug-cc-pVDZ basis set, at a lower computational cost.[49]

The pure electronic absorption and emission energies were computed by performing vertical $S_1 \leftarrow S_0$ and $S_1 \rightarrow S_0$ transitions from the ground- and the excited-state optimized geometries, respectively. For the absorption energies, the solvent effects were included by using the nonequilibrium PCM approach whereas in the case of emission energies the equilibrium and nonequilibrium PCM have been used to evaluate the energy of the excited and ground states, respectively.

Although, the absorption and emission energies have been computed by using both LR and SSPCM the excited state geometry optimizations in solution have been performed by using only the equilibrium LR implementation of PCM-TDDFT for which analytical gradients are available.[43]

It is worth to highlight that the maximum of an absorption or emission band does not necessarily coincide with the vertical energies, but it depends also on the Franck−Condon factors between the ground and the excited state minima and on the possible presence of vibronic interactions with close-lying excited states.[21,32,50,51]

However, since in this work we were more focused on the reproduction of the solvatochromic shifts and on the investigation of the formation of the TICT state, we decided to neglect the vibronic contribution (which cannot be computed at the SSPCM level) to the absorption and emission spectra as instead was done in previous investigations on coumarin molecules.[21,32]

dx.doi.org/10.1021/ct4004349 | J. Chem. Theory Comput. 2013, 9, 4087−4096

To investigate the formation of the TICT state of the C152 molecule, we have constructed the potential energy surfaces of the ground and the first singlet state (S_1) as function of the C−N dihedral angles (θ) by employing both the B3LYP and CAM-B3LYP functional.

Starting from the S_1 excited state optimized structure of the C152 molecule, successive conformations have been generated by varying the θ angle from 0° to 90° with a step size of 10°. For each conformation, all internal coordinates except the twisting angles of interest have been optimized by using the equilibrium LRPCM approach. Subsequently, the curves have been refined at the SSPCM level by employing the equilibrium and nonequilibrium regime for the S_1 and S_0 states, respectively.

Since the PCM alone is not able to reproduce well solvent effects for protic solvents, a mixed discrete-continuum approach was exploited to study the photophysical properties of C152 in water. In this case, two water molecules were placed near the carbonilic oxygen as shown in Figure 1.

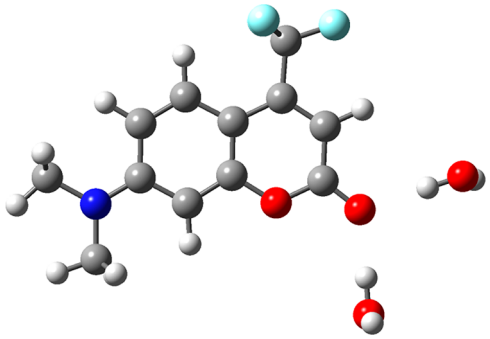

Figure 1. CAM-B3LYP/LRPCM optimized structure of the ground state C152 molecule with two explicit water molecules.

Finally, in all the PCM calculations, the cavity was computed by using the UFF atomic radii scaled by an α factor of 1.1 for every solvent, which is the default in Gaussian09. Improta et al. have shown that the VEEs of states with Sn character are affected by the dimension of the cavity (which depends on the α factor) rather than by the particular choice of the radii parametrization while the energy of Sπ states seems not affected by the cavity size.[52] However, a set of best α factor for each solvent has not been proposed yet and since a systematic investigation by using a large number of organic molecules belonging to different family compounds should be carried out; we decided to keep the original setting and not to employ different radii for different solvents.

RESULTS AND DISCUSSIONS

Solvent Effect on the Absorption and Emission Vertical Energies. The absorption ($S_1 \leftarrow S_0$) and emission ($S_1 \rightarrow S_0$) transition energies of C152 in cyclohexane, acetonitrile, and water solvents computed with the B3LYP and CAM-B3LYP functional by using the LRPCM and SSPCM approaches are reported in Table 1, together with their experimental counterparts previously published by Nad et al.[5]

Besides the vertical energies computed with B3LYP and CAM-B3LYP on the ground and excited state geometries optimized at the same level of theory, Table 1 also reports the same quantities computed with CAM-B3LYP on the B3LYP optimized structures. For simplicity, from now on all CAM-B3LYP calculations performed on the optimized structures at the B3LYP will be signed with an asterisk, CAM-B3LYP/LRPCM* or CAM-B3LYP/SSPCM*.

The experimental absorption spectrum of C152 is characterized by a single band, the maximum being centered at 3.23 (372 nm), 3.05 (393 nm), and 3.02 eV (398 nm) for CHX, ACN, and WAT, respectively.

Analysis of the orbital shapes confirms that the band is due to the first dipole-allowed $\pi \rightarrow \pi^*$ transition with the largest oscillator strength from the highest occupied molecular orbital (HOMO) to the lowest unoccupied molecular orbital (LUMO) depicted in Figure 2. The HOMO is delocalized on the whole molecule, with significant contribution by the π orbitals of the "central" benzenic ring and the orbitals localized on the N,N-dialkyl group. The LUMO is mainly localized on the "quinonelike" terminal ring with significant contribution of

Table 1. Absorption and Emission Energies (in eV) and Oscillator Strengths (in Parentheses) of C152 in Cyclohexane (CHX), Acetonitrile (ACN), and Water (WAT) Solvent Computed by Employing the LRPCM and SSPCM with Different Density Functional[a]

	abs. (eV)			emi. (eV)			Stokes' shift		
B3LYP	LRPCM	SSPCM	exp.	LRPCM	SSPCM	exp.	LRPCM	SSPCM	exp.
CHX	3.21(0.46)	3.07(0.33)	3.23	2.81(0.35)	2.57(0.25)	2.81	0.40	0.50	0.42
ACN	3.09(0.42)	2.81(0.33)	3.05	2.60(0.50)	2.22(0.26)	2.38	0.49	0.59	0.67
WAT	2.97(0.43)	2.80(0.33)	3.02	2.50(0.48)	2.18(0.26)	2.34	0.47	0.62	0.68
	abs. (eV)			emi. (eV)			Stokes' shift		
CAM-B3LYP	LRPCM	SSPCM	exp.	LRPCM	SSPCM	exp.	LRPCM	SSPCM	exp.
CHX	3.70(0.70)	3.59(0.46)	3.23	3.28(0.59)	3.21(0.46)	2.81	0.42	0.38	0.42
ACN	3.58(0.58)	3.32(0.46)	3.05	2.98(0.77)	2.82(0.47)	2.38	0.60	0.50	0.67
WAT	3.43(0.58)	3.27(0.47)	3.02	2.87(0.75)	2.76(0.46)	2.34	0.56	0.51	0.68
	abs. (eV)			emi. (eV)			Stokes' shift		
CAM-B3LYP[b]	LRPCM	SSPCM	exp.	LRPCM	SSPCM	exp.	LRPCM	SSPCM	exp.
CHX	3.61(0.60)	3.52(0.46)	3.23	3.29(0.49)	3.06(0.37)	2.81	0.32	0.46	0.42
ACN	3.48(0.59)	3.25(0.47)	3.05	3.01(0.66)	2.55(0.38)	2.38	0.47	0.70	0.67
WAT	3.35(0.58)	3.19(0.47)	3.02	2.91(0.65)	2.47(0.38)	2.34	0.44	0.72	0.68

[a]The experimental values reported in the literature are also listed. [b]Calculations performed on the geometric structure optimized at the B3LYP/LRPCM level.

dx.doi.org/10.1021/ct4004349 | J. Chem. Theory Comput. 2013, 9, 4087−4096

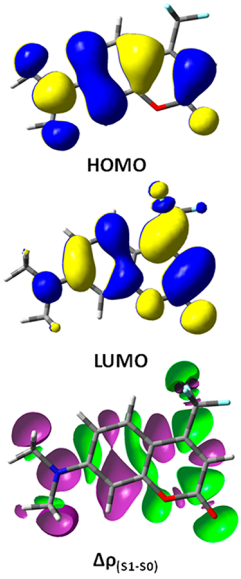

Figure 2. Kohn–Sham MOs involved during the $S_1 \leftarrow S_0$ and the electron density change ($\Delta\rho_{S1-S0}$) upon absorption of light for C152 in acetonitrile. Light green clouds represent regions in which the electron density increases during the transition; dark violet clouds represent regions in which the electron density decreases during the transition.

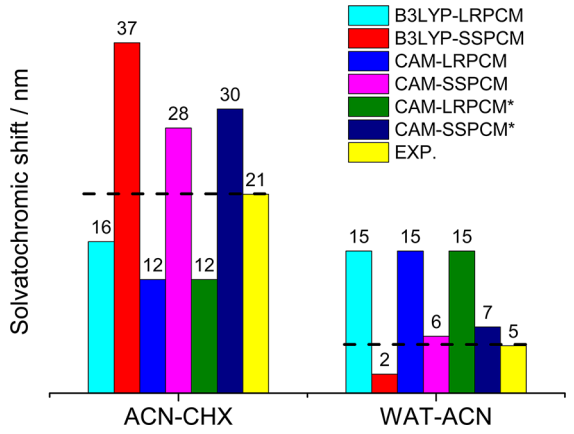

Figure 3. Solvatochromic shifts between ACN-CHX and WAT-ACN computed with different functional and PCM approaches for the $S_1 \leftarrow S_0$ transition.

the π^* orbital of the carbonyl group and of a partial π bond between the aromatic carbon and the CF_3 group.

Consequently, the $S_1 \leftarrow S_0$ transition has a partial intramolecular charge transfer character from the N-alkyl groups to the carbonyl and CF_3 groups, as also evidenced by looking at the electron density difference, also reported in Figure 2, between the excited and the ground states ($\Delta\rho_{S1-S0}$) upon light absorption. The light green clouds represents positive regions (regions in which the electron density increases during the transition) and dark violet the clouds negative regions (in which the electron density decreases during the transition). Therefore, the electron density on the carbonyl and on the CF_3 moieties is enhanced at the expense of the electron density on the N-alkyl group after the HOMO–LUMO orbital transition.

The results show that both LRPCM and SSPCM approaches well reproduce the red shift with the increasing solvent polarity (Table 1). In general, the ACN-CHX solvatochromic shift is slightly underestimated by LRPCM, slightly overestimated by SSPCM, whereas the WAT-ACN shift is slightly overestimated by LRPCM and very well reproduced by SSPCM (Figure 3). Interestingly, the CAM-B3LYP/SSPCM approach gives very good solvatochromic shifts on both CAM-B3LYP and B3LYP optimized ground state structures. This is a consequence of the similarity among the two ground state geometries, which present a planar 7-N,N-dialkyl-amino group with almost identical bond lengths and angles, and in resonance with the benzopyrone moiety.

A single band (Table 1) also characterizes the emission spectra. The experimental data[5] show that the Stoke's shifts ($\Delta\lambda_S$) correlate linearly with the polarity parameter of the solvents, even though for nonpolar solvents the Stoke's shift is unusually lower. In fact, it is 55 nm for CHX and 111 and 115 for ACN and WAT, respectively.

This peculiarity was attributed to a different nature of the ground and excited states of C152 in nonpolar solvents; in particular, to the existence of "nonpolar structures" with a pyramidal configuration of the 7-N,N-alkyl amino group[5] and, consequently, out of resonance with the benzopyrone moiety.

The comparison between the experimental and computed data (Table 1) demonstrates unequivocally that LRPCM is not sufficient to reproduce correctly the large Stokes' shift of organic molecules having a large excited state dipole moment in polar solvents. Better results are obtained when the B3LYP/SSPCM approach is used. Surprisingly, B3LYP/SSPCM and CAM-B3LYP/SSPCM calculations on the respective optimized excited state geometries present very different results. While the Stokes' shifts computed at the B3LYP/SSPCM level of theory are in fairly agreement with experiments, the Stoke's shifts computed with CAM-B3LYP/SSPCM on the S_1 structure optimized at the same level of theory are heavily underestimated. The inspection of the excited state optimized structures reveals that these differences are due to a very different behavior of the B3LYP/LRPCM and CAM-B3LYP/LRPCM approaches during the excited state geometry minimizations.

As shown by the data reported in Table 2, both geometries present a planar structure with the twisting and pyramidalization angles on the amino group equal to zero, independently on the polarity of the solvent. Therefore, the interpretation furnished by Nad et al.[5] concerning the small Stokes' shift of C152 in nonpolar solvent cannot be confirmed; this effect may instead simply be due to the solvent reaction field.

Significant differences in the optimized geometries are found for the C–N and C=O bond lengths as reported in Table 2. In particular, B3LYP calculations predict an increase of both bonds upon the ground to excited state transition, whereas CAM-B3LYP shows a decrease of the C–N bond and an increase of the C=O bond. Therefore, as already reported for the dye "Nile Red"[40] the results of B3LYP/LRPCM suggest that the CN bond has a larger single bond character in the excited state than in the ground state, while for CAM-B3LYP/LRPCM calculations the CN bond gain a more market double bond character in the excited state.

Since CAM-B3LYP/SSPCM calculations on the CAM-B3LYP/LRPCM optimized structure provide poor emission energies, we have decided to perform CAM-B3LYP/SSPCM single point calculations on the B3LYP/LRPCM optimized S_1 structure (denoted by CAM-B3LYP/SSPCM*).

dx.doi.org/10.1021/ct4004349 | J. Chem. Theory Comput. 2013, 9, 4087–4096

Table 2. C−N and C═O Bond Lengths (in Å) and Twisting and Pyramidalization Angles (in Degrees) for the S_1 Excited and S_0 Ground States (in Parentheses) at the B3LYP/LRPCM and CAM-B3LYP/LRPCM Level of Theory

	B3LYP			CAM-B3LYP		
	CHX	ACN	WAT	CHX	ACN	WAT
C═O	1.23 (1.21)	1.24 (1.22)	1.25 (1.24)	1.22 (1.21)	1.23 (1.22)	1.25 (1.24)
C−N	1.39 (1.37)	1.38 (1.36)	1.38 (1.36)	1.36 (1.37)	1.35 (1.36)	1.35 (1.36)
θ	0 (0)	0 (0)	2.6 (0)	0 (0)	0 (0)	0.7 (0)
δ	0 (0)	0 (0)	0.1 (0)	0 (0)	0 (0)	0.1 (0)

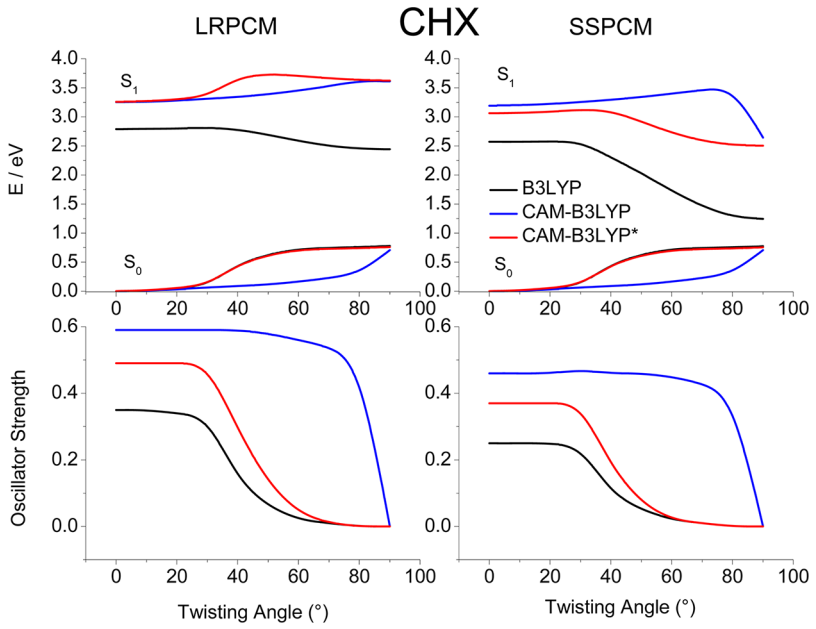

Figure 4. Potential energy curves and oscillator strength for the $S_1 \rightarrow S_0$ transition as a function of the twisting angle θ of the C152 molecule computed at the LRPCM (left) and SSPCM (right) levels by employing the B3LYP and CAM-B3LYP functional in cyclohexane. CAM-B3LYP* stands for CAM-B3LYP calculations performed on the B3LYP/LRPCM optimized structures.

The Stokes' shifts obtained by CAM-B3LYP/SSPCM* calculations, reported in Table 1, are in perfect agreement with the experimental ones.

The single point CAM-B3LYP/SSPCM calculations performed on the B3LYP and CAMB3LYP S_1 minima show that the formers are more stable of 12.38, 0.16, and 0.15 eV in CHX, ACN, and WAT solutions, respectively.

The electronic transitions on the two minima involve the same orbitals even though a major electronic contribution is transferred from the N,N-alkyl amino group to the CO moiety as evidenced also by the excited state dipole moments which are slightly larger on the B3LYP geometries. These increase with the solvent polarity from 15.44 (14.33 on the CAM-B3LYP geometry) to 18.00 (17.18) and 21.07 D (20.08) for CHX, ACN, and WAT, respectively.

Overall, the B3LYP/LRPCM geometries seem to be more reliable than the CAM-B3LYP/LRPCM ones.

In light of these results, two points are worth of further comments: (1) it is known[53] that the B3LYP functional overestimates the stability of the charge-transfer states (as it is that of the C152); therefore, one might wonder which is the rational of using the B3LYP/LRPCM geometry of the excited state; (2) LRPCM underestimates the energy of solvation between solute and solvent especially if the latter is polar.[41,42] Therefore, LRPCM is not the appropriate approach to describe the effect of the solvent for an excited solute as also demonstrated by the results on the Stokes shift discussed earlier.

For these reasons, the most appropriate level to treat this problem would be the CAM-B3LYP/SSPCM one, but the geometry optimization at this level is not affordable yet.

Instead, a B3LYP/LRPCM excited state optimization could lead to a reasonable geometry for a simple '*error cancellation*' effect, as it seems to happen in this case.

Twisted Intramolecular Charge Transfer State: LRPCM vs SSPCM. Previous fluorescence spectroscopic measurements showed that the fluorescence quantum yield and lifetimes of C152 are quite high for nonpolar solvents but undergo a drastic reduction in highly polar solvents.[5,10] These results were attributed to the formation of a nonemissive twisted intramolecular charge transfer state in polar solvents. According to this deactivation mechanism, the rotation (by 90°) of the 7-N,N-dialkylamino group with respect to the benzopyrone moiety leads to a zwitterionic structure (in which the nitrogen atom bears a positive charge whereas the negative charge is delocalized on the 1,2-benzopyrone moiety); and thus, it is expected to be more stabilized in polar solvents.

The formation of the TICT state in 7-aminocoumarin molecules has never been theoretically confirmed. Therefore, to gain new insights into the more probable deactivation decay mechanism of the C152 molecule, the potential energy surfaces of the ground and the first singlet (S_1) states as function of the twisting C−N dihedral angles (θ) have been computed by

dx.doi.org/10.1021/ct4004349 | J. Chem. Theory Comput. 2013, 9, 4087−4096

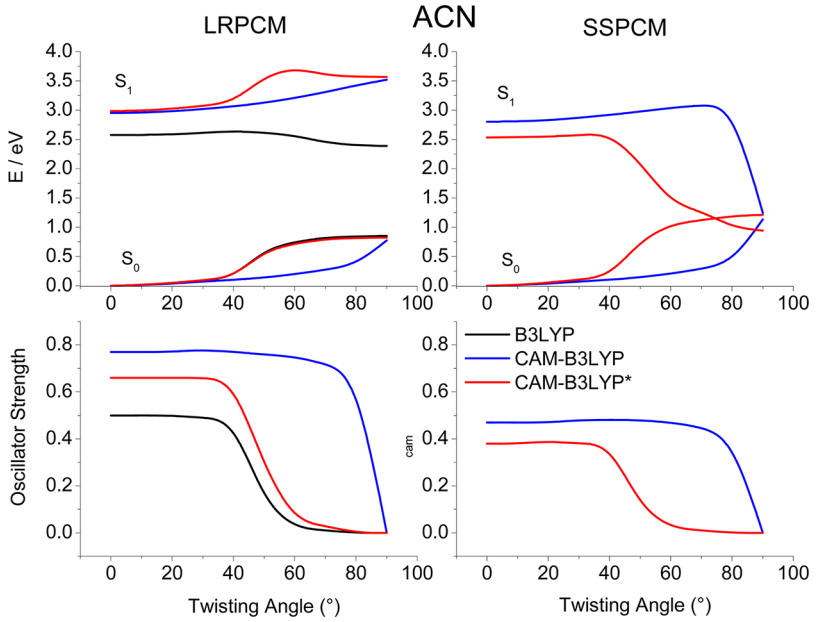

Figure 5. Potential energy curves and oscillator strength for the $S_1 \rightarrow S_0$ transition as a function of the twisting angle θ of the C152 molecule computed at the LRPCM (left) and SSPCM (right) levels by employing the B3LYP and CAM-B3LYP functional in acetonitrile. CAM-B3LYP* stands for CAM-B3LYP calculations performed on the B3LYP/LRPCM optimized structures. B3LYP/SSPCM PESs have not been reported because for twisting angles between 70 and 90° the State-Specific PCM does not reach self-consistency.

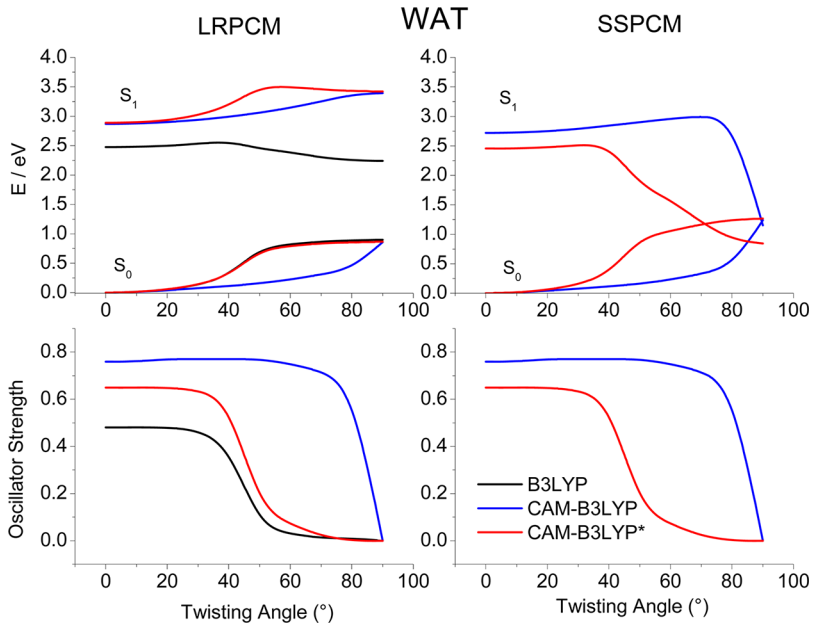

Figure 6. Potential energy curves and oscillator strength for the $S_1 \rightarrow S_0$ transition as a function of the twisting angle θ of the C152 molecule computed at the LRPCM (left) and SSPCM (right) levels by employing the B3LYP and CAM-B3LYP functional in water. CAM-B3LYP* stands for CAM-B3LYP calculations performed on the B3LYP/LRPCM optimized structures. B3LYP/SSPCM PESs have not been reported because for twisting angles between 70 and 90° the State-Specific PCM does not reach self-consistency.

employing the B3LYP and CAM-B3LYP functionals in combination with LRPCM and SSPCM.

Figures 4, 5, and 6 report the potential energy curves together with the oscillator strength for the $S_1 \rightarrow S_0$ transition as a function of the θ angle for C152 in CHX, ACN, and WAT solutions, respectively.

Figure 4 shows that the twist of the θ angle has a strong effect on the oscillator strength, which smoothly tends to zero at 90° for both B3LYP/LRPCM and CAM-B3LYP/LRPCM calculations on the B3LYP optimized structures, while a negligible effect is observed on the CAM-B3LYP/LRPCM optimized structure.

As it can be noted, when the solvent is treated at the LRPCM level B3LYP and CAM-B3LYP* calculations are the only ones that provide a second minimum at 90° while CAM-B3LYP/LRPCM calculations do not detect a TICT stable structure.

The TICT state is assigned to the excitation of an electron localized on the 7-alkylamino substituent to the "quinonelike" terminal ring with a significant contribution of the π^* orbital of

dx.doi.org/10.1021/ct4004349 | J. Chem. Theory Comput. 2013, 9, 4087−4096

the carbonyl group, as shown by the HOMO−LUMO Khon-Sham molecular orbitals reported in Figure 7.

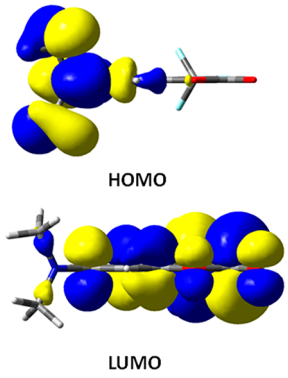

Figure 7. Kohn−Sham MOs involved in the TICT state of the C152 molecule in ACN.

The B3LYP/LRPCM PES shows that the two minima at a twist angles of 0° and 90° corresponding to the ICT and TICT states are connected by a small rotation barrier of 2.58 kJ/mol whereas the CAM-B3LYP/LRPCM* curve shows that the two minima are separated by a very large energy barrier of about 48.2 kJ/mol.

The TICT state is also detected (although at a much higher energy) by the CAM-B3LYP/SSPCM calculations, but a very high energy barrier (about 30.2 kJ/mol) between the ICT and the TICT states is detected. Therefore, based on these results, the TICT state should not be populated at room temperature. However, Figure 4 also shows that CAM-B3LYP/SSPCM* calculations produces quite different results: the rotation energy barrier decreases to 5.8 kJ/mol and the twisted structure becomes more stable than the planar one by about 0.56 eV. The gap between the ground and excited states is larger than 1.7 eV and thus internal conversion processes do not seem to be favorite.

These results suggest that CAM-B3LYP/SSPCM geometry optimizations would lead to different structures with respect to that obtained by using CAM-B3LYP/LRPCM because LRPCM calculations underestimate the energy of solvation when the solute is in an excited state with charge transfer (CT) character.

The same PESs computed in acetonitrile and water solvents are reported in Figures 5 and 6. A marked similarity of the shapes of the curves to that computed in cyclohexane is observed when the LRPCM approach is used. That is, the TICT state is detected only by B3LYP and CAMB3LYP* calculations. However, a different behavior is observed for SSPCM calculations. In particular, a crossing between the S_1 and S_0 PESs is observed by both CAM-B3LYP/SSPCM and CAM-B3LYP/SSPCM* calculations at around 90 and 70°, respectively. Once again, these results demonstrate that CAM-B3LYP/LRPCM and CAM-B3LYP/SSPCM geometry optimizations would lead to different excited state structures since they yield different PES on the twisted B3LYP/LRPCM optimized structures.

To further analyze the nature of the two minima at the twist angle of 0° and 90°, the charge transfer parameter proposed by Guido et al.[40] has been computed for the different solvents on the B3LYP and CAM-B3LYP minima and reported in Table 3. The parameter is defined as $f_{CT} = \Delta q_D - \Delta q_A$, where Δq_i is the charge difference (the Merz−Kollman[54] charges have been used in this work) in the donor or acceptor unit between ground and excited state. The donor and acceptor groups are the N,N-dialkyl group and the CO moiety. If the excitation really corresponds to a CT from donor to acceptor, f_{CT} will be large and positive since Δq_D is large and positive while Δq_A is large in absolute value but negative.

Table 3. Charge Transfer Parameters (f_{CT}) Computed at the CAM-B3LYP/SSPCM Level of Theory on the Planar (θ = 0°) and Twisted (θ = 90°) CAM-B3LYP and B3LYP (CAM-B3LYP*) Geometries

	CAM-B3LYP		CAM-B3LYP*	
	0°	90°	0°	90°
CHX	0.19	0.67	0.21	0.63
ACN	0.23	0.71	0.30	0.63
WAT	0.28	0.70	0.32	0.66

The table clearly shows that both the B3LYP and CAM-B3LYP minima at the twisting angle of 90° have larger CT parameters thus supporting the hypothesis of a TICT process, which seems more probable with increasing the solvent polarity.

Therefore, as we have very recently shown for 7-diethylaminocoumarin-3-carboxylic acid derivative molecules,[55] CAM-B3LYP/SSPCM* calculations suggest that the formation of a TICT state and the intersection between the S_1 and S_0 adiabatic PESs is responsible for the reduced fluorescence quantum yield of **C152** molecule in polar solvents. Upon excitation from the ground state structure, the Franck−Condon or locally excited state with a weak intramolecular charge transfer character is reached, but an equilibrium between the ICT and TICT states can be established at room temperature since the energy barrier of rotation is a few kJ/mol (6.7 and 6.1 kJ/mol in ACN and WAT, respectively). For nonpolar solvent, the formation of the TICT state does not necessarily leads to a fast nonradiative deactivation as it happens in polar solvents because the crossing among the S_0 and S_1 curves does not seem to occur.

CONCLUSIONS

The electronic excited states involved in the absorption an emission spectra of C152 in solvents with different polarity have been investigated by using time-dependent density functional theory and PCM calculations.

The possible formation of a TICT state for the C152 molecule have been assessed by computing the PESs of the ground and the first singlet excited state (S_1) as function of the twisting C−N dihedral angles by employing the B3LYP and CAM-B3LYP functional in combination with LRPCM and SSPCM to account for the effects of solvent with different polarities. It turned out that the combination among the functional and the PCM models used has a major impact on the results obtained.

Whereas both B3LYP and CAM-B3LYP calculations coupled with the SSPCM model provide good solvatochromic shifts on the absorption energies they give very different Stokes' shifts.

This is a consequence of the different three-dimensional structures obtained by means of B3LYP/LRPCM and CAM-B3LYP/LRPCM approaches. Although both geometries present a planar structure independently on the solvent and the MOs involved during the transitions are the same, more significant variations are found for the C−N and C═O bonds. B3LYP/LRPCM calculations suggest that the CN bond has a

dx.doi.org/10.1021/ct4004349 | J. Chem. Theory Comput. 2013, 9, 4087−4096

larger single bond character in the excited state than in the ground state, while for CAM-B3LYP/LRPCM calculations the CN bond gain a more market double bond character in the excited state.

The very good agreement with experimental Stokes' shifts found when the emission energies are computed at the CAM-B3LYP/SSPCM level of theory on the B3LYP/LRPCM geometries suggests that the balance between the over-polarization error of B3LYP for charge transfer states and the underestimation of solvation energy of LRPCM for CT excited states in polar solvents can lead to reasonable excited state geometries thanks to an error cancellation effect. On the contrary, CAM-B3LYP/LRPCM geometry optimizations could be misleading for CT states in polar solvents.

This has been confirmed by investigating the S_1 potential energy surface of C152 as a function of the twisting angle around the C−N bond. In fact, the potential energy surfaces obtained by using CAM-B3LYP/SSPCM on B3LYP/LRPCM optimized structures are very different to that obtained by using CAM-B3LYP/LRPCM. The former calculations show the formation of a twisted intramolecular charge transfer state at the twisting angle of around 70°, while the latter ones reveal a very high-energy barrier among the ICT and the TICT states. Therefore, a CAM-B3LYP/SSPCM optimization would lead to geometries different than the one obtained with CAM-B3LYP/LRPCM.

Finally, our calculations have allowed us to interpret the unusual photophysical behavior of C152 in nonpolar and in highly polar solvents. CAM-B3LYP/SSPCM* calculations show that the twisted intramolecular charge transfer state forms in all the investigated solvents but only in polar solvent the crossing between the S_1 and S_0 states can lead to fast nonradiative de-excitation and thus to quantum yields and lifetimes drastically reduced.

AUTHOR INFORMATION

Corresponding Author

*E-mail: alfonso.pedone@unimo.it.

Notes

The authors declare no competing financial interest.

ACKNOWLEDGMENTS

Financial support is acknowledged from the Italian Minister of University and research (MIUR) through the FIRB Futuro in Ricerca project entitled "Novel Multiscale Theoretical/Computational Strategies for the Design of Photo and Thermo Responsive Hybrid Organic−Inorganic Composites for Nano-electronic Circuits" (Contract No. RBFR1248UI)

REFERENCES

(1) Sheats, J. R.; Barbara, P. F. Molecular Materials in Electronic and Optoelectronic Devices. *Acc. Chem. Res.* **1999**, *32*, 191−192.

(2) Yang, Y. S.; Zou, J.; Rong, H.; Qian, G. D.; Wang, z. Y.; Wang, M. Q. Inflence of Various Coumarin Dyes on the Laser Preformance of Laser Dyes Co-doped into ORMOSILs. *Appl. Phys. B: Laser Opt.* **2007**, *86*, 309−313.

(3) Kozlov, V. G.; Parthasarathy, G.; Burrows, P. E.; Forrest, S. R. Optically Pumped Blue Organic Semiconductor Lasers. *Appl. Phys. Lett.* **1998**, *72*, 144−146.

(4) Schulz-Ekloff, G.; Wöhrle, D.; van Duffel, B.; Schoonheydt, R. A. Chromophores in Porous Silicas and Minerals: Preparation and Optical Properties. *Microporous Mesoporous Mater.* **2002**, *51*, 91−138.

(5) Nad, S.; Kumbhakar, M.; Pal, H. Photophysical Properties of Coumarin-152 and Coumarin-481 Dyes: Unusual Behavior in Nonpolar and in Higher Polarity Solvents. *J. Phys. Chem. A* **2003**, *107*, 4808−4816.

(6) Nad, S.; Pal, H. Unusual Photophysical Properties of Coumarin-151. *J. Phys. Chem. A* **2001**, *105*, 1097−1106.

(7) Wagner, B. D. The Use of Coumarins as Environmentally-Sensitive Fluorescent Probes of Heterogeneous Inclusion Systems. *Molecules* **2009**, *14*, 210−237.

(8) Jones, G. I.; Jackson, W. R.; Choi, C.; Bergmark, W. R. Solvent Effects on Emission Yield and Lifetime for Coumarin Laser Dyes. Requirements for a Rotatory Decay Mechanism. *J. Phys. Chem.* **1985**, *89*, 294−300.

(9) Jones, G. I.; Jackson, W. R.; Kanoktanaporn, S.; Halper, A. M. Solvent Effects on Photophysical Parameters for Coumarin Laser Dyes. *Opt. Commun.* **1980**, *33*, 315−320.

(10) Dahiya, P.; Kumbhakar, M.; Mukherjee, T.; Pal, H. Effect of Protic Solvents on Twisted Intramolecular Charge Transfer State Formation in Coumarin-152 and Coumarin-481 Dyes. *Chem. Phys. Lett.* **2005**, *414*, 148−154.

(11) Satpati, A. K.; Kumbhakar, M.; Nath, A.; Pal, H. Photophysical Properties of Coumarin-7 Dye: Role of Twisted Intramolecular Charge Transfer State in High Polarity Protic Solvents. *Photochem. Photobiol.* **2009**, *85*, 119−129.

(12) Rechthaler, K.; Köhler, G. Excited State Properties and Deactivation Pathways of 7 Aminocoumarins. *Chem. Phys.* **1994**, *189*, 99116.

(13) Runge, E.; Gross, E. K. U. Density-Functional Theory for Time-Dependent Systems. *Phys. Rev. Lett.* **1984**, *52*, 997−1000.

(14) Dreuw, A.; Head-Gordon, M. Single-Reference Ab Initio Methods for the Calculation of Excited States of Large Molecules. *Chem. Rev.* **2005**, *105*, 4009−4037.

(15) Mennucci, B. Modeling Environment Effects on Spectroscopies Through QM/Classical Models. *Phys. Chem. Chem. Phys.* **2013**, *15*, 6583−6594.

(16) Pedone, A.; Prampolini, G.; Monti, S.; Barone, V. Absorption and Emission Spectra of Fluorescent Silica Nanoparticles from TD-DFT/MM/PCM Calculations. *Phys. Chem. Chem. Phys.* **2011**, *13*, 16689−16697.

(17) Adamo, C.; Jacquemin, D. The Calculations of Excited-State Properties with Time-Dependent Density Functional Theory. *Chem. Soc. Rev.* **2013**, *42*, 845−856.

(18) Jacquemin, D.; Mennucci, B.; Adamo, C. Excited-State Calculations with TD-DFT: from Benchmarks to Simulations in Complex Environments. *Phys. Chem. Chem. Phys.* **2011**, *13*, 16987−16998.

(19) Pedone, A.; Barone, V. Unraveling Solvent Effects on the Electronic Absorption Spectra of TRITC Fluorophore in Solution: A Theoretical TD-DFT/PCM Study. *Phys. Chem. Chem. Phys.* **2010**, *12*, 2722−2729.

(20) Pedone, A.; Biczysko, M.; Barone, V. Environmental Effects in Computational Spectroscopy: Accuracy and Interpretations. *ChemPhysChem* **2010**, *11*, 1812−1832.

(21) Pedone, A.; Bloino, J.; Barone, V. Role of Host-Guest Interactions in Tuning the Optical Properties of Coumarin Derivatives Incorporated in MCM-41: A TD-DFT Investigation. *J. Phys. Chem. C* **2012**, *116*, 17807−17818.

(22) Pedone, A.; Bloino, J.; Monti, S.; Prampolini, G.; Barone, V. Absorption and Emission UV−Vis Spectra of the TRITC Fluorophore Molecule in Solution: A Quantum Mechanical Study. *Phys. Chem. Chem. Phys.* **2010**, *12*, 1000−1006.

(23) Pedone, A.; Prampolini, G.; Monti, S.; Barone, V. Realistic Modelling of Fluorescent Dye-Doped Silica Nanoparticles: A Step Toward the Understanding of their Enhanced Photophysical Properties. *Chem. Mater.* **2011**, *23*, 5016−5023.

(24) Jacquemin, D.; Planchat, A.; Adamo, C.; Mennucci, B. TD-DFT Assessment of Functionals for Optical 0−0 Transitions in Solvated Dyes. *J. Chem. Theory Comput.* **2012**, *8*, 2359−2372.

(25) Labat, F.; Ciofini, I.; Hratchian, H. P.; Frisch, M. J.; Raghavachari, K.; Adamo, C. First-Principles Modeling of Eosin-Loaded ZnO Films: A Step Toward the Understanding of Dye-

Sensitized Solar Cell Performances. *J. Am. Chem. Soc.* **2009**, *131*, 14290−14298.
(26) De Angelis, F.; Tilocca, A.; Selloni, A.; Time-Dependent, D. F. T. Study of $[Fe(CN)_6]_4^-$ Sensitization of TiO_2 Nanoparticles. *J. Am. Chem. Soc.* **2004**, *126*, 15024−15025.
(27) Sakata, T.; Kawashima, Y.; Nakano, H. Low-Lying Excited States of C120 and C151: A Multireference Perturbation Theory Study. *J. Phys. Chem. A* **2010**, *114*, 12363−12368.
(28) Jacquemin, D.; Perpète, E. A.; Assfeld, X.; Scalmani, G.; Frisch, M.; Adamo, C. The Geometries, Absorption, and Fluorescence Wavelengths of Solvated Fluorescent Coumarins: A CIS and TD-DFT Comparative Study. *Chem. Phys. Lett.* **2007**, *438*, 208−212.
(29) Kurashige, Y.; Nakajima, T.; Kurashige, S.; Hirao, K.; Nisikitani, Y. Theoretical Investigation of the Excited States of Coumarin Dyes for Dye-Sensitized Solar Cells. *J. Phys. Chem. A* **2007**, *111*, 5544−5548.
(30) Zhao, W.; Bian, w. Investigation of the Structures and Electronic Spectra for Coumarin 6 through TD-DFT Calculations Including PCM Solvation. *J. Mol. Struct.: THEOCHEM* **2007**, *818*, 43−49.
(31) Wu, W.; Cao, Z.; Zhao, Y. Theoretical Studies on Absorption, Emission, and Resonance Raman Spectra of Coumarin 343 Isomers. *J. Chem. Phys.* **2012**, *136*, 114305−114313.
(32) Improta, R.; Barone, V.; Santoro, F. Ab Initio Calculations of Absorption Spectra of Large Molecules in Solution: Coumarin C153. *Angew. Chem., Int. Ed.* **2007**, *46*, 405−408.
(33) Zhao, W.; Ding, Y.; Xia, Q. Time-Dependent Density Functional Theory Study on the Absorption Spectrum of Coumarin 102 and Its Hydrogen-Bonded Complexes. *J. Comput. Chem.* **2011**, *32*, 545−553.
(34) Miao, C.; Shi, Y. Reconsideration on Hydrogen Bond Strengthening or Cleavage of Photoexcited Coumarin 102 in Aqueous Solvent: A DFT/TDDFT Study. *J. Comput. Chem.* **2011**, *32*, 3058−3061.
(35) Becke, A. D. A New Mixing of Hartree-Fock and Local Density-Functional Theories. *J. Chem. Phys.* **1993**, *98*, 5648−5652.
(36) Adamo, C.; Barone, V. Toward Reliable Density Functional Methods Without Adjustable Parameters: The PBE0Model. *J. Chem. Phys.* **1999**, *110*, 6158−6169.
(37) Tomasi, J.; Mennucci, B.; Cammi, R. Quantum Mechanical Continuum Solvation Models. *Chem. Rev.* **2005**, *105*, 2999−3094.
(38) Chiba, M.; Tsuneda, T.; Hirao, K. Long-Range Corrected Time-Dependent Density Functional Study on Fluorescence of 4,4′-Dimethylaminobenzonitrile. *J. Chem. Phys.* **2007**, *126*, 034504.
(39) Wiggins, P.; Gareth Williams, J. A.; Tozer, D. J. Excited State Surfaces in Density Functional Theory: A New Twist on an Old Problem. *J. Chem. Phys.* **2009**, *131*, 091101.
(40) Guido, C.; Mennucci, B.; Jacquemin, D.; Adamo, C. Planar vs Twisted Intramolecular Charge Transfer Mechanism in Nile Red: New Hints from Theory. *Phys. Chem. Chem. Phys.* **2010**, *12*, 8016−8023.
(41) Improta, R.; Scalmani, G.; Frisch, M.; Barone, V. Toward Effective and Reliable Fluorescence Energies in Solution by New State Specific Polarizable Continuum Model time Dependent Density Functional Theory Approach. *J. Chem. Phys.* **2007**, *127*, 074504.
(42) Improta, R.; Barone, V.; Scalmani, G.; Frisch, M. A State-Specific Polarizable Continuum Model Time Dependent Density Functional Theory Method for Excited State Calculations in Solution. *J. Chem. Phys.* **2006**, *125*, 054103.
(43) Scalmani, G.; Frisch, M.; Mennucci, B.; Tomasi, J.; Cammi, R.; Barone, V. Geometries and Properties of Excited States in the Gas Phase and in Solution: Theory and Application of a Time-Dependent Density Functional Theory Polarizable Continuum Model. *J. Chem. Phys.* **2006**, *124*, 094107.
(44) Improta, R.; Barone, V.; Santoro, F. Accurate Steady State and Zero Time Fluorescence Spectra of Large Molecules in Solution by a First Principle Computational Method. *J. Phys. Chem. B* **2007**, *111*, 14080−14082.
(45) Improta, R. The Excited States of p-Stacked 9-Methyladenine Oligomers: A TD-DFT Study in Acqueous Solution. *Phys. Chem. Chem. Phys.* **2008**, *10*, 2656−2664.
(46) Frisch, M. J. T., G. W.; Schlegel, H. B.; Scuseria, G. E.; Robb, M. A.; Cheeseman, J. R.; Scalmani, G.; Barone, V.; Mennucci, B.; Petersson, G. A.; Nakatsuji, H.; Caricato, M.; Li, X.; Hratchian, H. P.; Izmaylov, A. F.; Bloino, J.; Zheng, G.; Sonnenberg, J. L.; Hada, M.; Ehara, M.; Toyota, K.; Fukuda, R.; Hasegawa, J.; Ishida, M.; Nakajima, T.; Honda, Y.; Kitao, O.; Nakai, H.; Vreven, T.; Montgomery, Jr., J. A.; Peralta, J. E.; Ogliaro, F.; Bearpark, M.; Heyd, J. J.; Brothers, E.; Kudin, K. N.; Staroverov, V. N.; Kobayashi, R.; Normand, J.; Raghavachari, K.; Rendell, A.; Burant, J. C.; Iyengar, S. S.; Tomasi, J.; Cossi, M.; Rega, N.; Millam, N. J.; Klene, M.; Knox, J. E.; Cross, J. B.; Bakken, V.; Adamo, C.; Jaramillo, J.; Gomperts, R.; Stratmann, R. E.; Yazyev, O.; Austin, A. J.; Cammi, R.; Pomelli, C.; Ochterski, J. W.; Martin, R. L.; Morokuma, K.; Zakrzewski, V. G.; Voth, G. A.; Salvador, P.; Dannenberg, J. J.; Dapprich, S.; Daniels, A. D.; Farkas, Ö.; Foresman, J. B.; Ortiz, J. V.; Cioslowski, J.; Fox, D. J. . *Gaussian09*, Revision A.1 ed.; Gaussian, Inc.: Wallingford, CT, 2009.
(47) Lee, C.; Yang, W.; Parr, R. G. Developement of the Colle−Salvetti Correlation-Energy Formula into a Functional of the Electron Density. *Phys. Rev. B* **1988**, *37*, 785−789.
(48) Tawada, Y.; Tsuneda, T.; Yanagisawa, S.; Yanai, T.; Hirao, K. A Long-Range Corrected Time-Dependent Density Functional Theory. *J. Chem. Phys.* **2004**, *120*, 8425−8433.
(49) Barone, V.; Cimino, P. Accurate and Feasible Computations of Structural and Magnetic Properties of Large Free Radicals: The PBE0/N07D Model. *Chem. Phys. Lett.* **2008**, *454*, 139−143.
(50) Bloino, J.; Biczysko, M.; Santoro, F.; Barone, V. General Approach to Compute Vibrationally Resolved One-Photon Electronic Spectra. *J. Chem. Theory Comput.* **2010**, *6*, 1256−1274.
(51) Santoro, F.; Improta, R.; Lami, A.; Bloino, J.; Barone, V. Effective Method to compute Franck−Condon Integrals for Optical Spectra of Large Molecules in Solution. *J. Chem. Phys.* **2007**, *126*, 084509.
(52) Improta, R.; Barone, V. PCM/TD-DFT Study of the Two Lowest Excited States of Uracil Derivatives in Solution: The Effect of the Functional and of the Cavity Model. *J. Molec. Struct.: THEOCHEM* **2009**, *914*, 87−93.
(53) Peach, M. J. G.; Benfield, P.; Helhgaker, T.; Tozer, D. J. Excitation Energies in Density Functional Theory: An Evaluation and a Diagnostic Test. *J. Chem. Phys.* **2008**, *128*, 044118.
(54) Besler, B. H.; Merz, K. M.; Kollman, P. Atomic Charges Derived from Semiempirical Methods. *J. Comput. Chem.* **1990**, *11*, 431−439.
(55) Pedone, A.; Gambuzzi, E.; Barone, V.; Bonacchi, S.; Genovese, D.; Rampazzo, E.; Prodi, L.; Montalti, M. Understanding the Photophysical Properties of Coumarin-based Pluronic-Silica (PluS) Nanoparticles by Means of Time-Resolved Emission Spectroscopy and Accurate TDDFT/Stochastic Calculations. *Phys. Chem. Chem. Phys.* **2013**, *15*, 12360−12372.